energyequipsys/ Vol 3/No1/Jan 2015/ 45-56

ENERGY EQUIPSYS

Energy Equipment and Systems

http://energyequipsys.ut.ac.ir

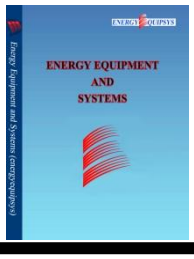

Numerical aeroelastic analysis of wind turbine NREL Phase VI Rotor

Authors

Edris Bagheri[a]
Amir Nejat[b*]

[a] School of Mechanical Engineering, Alborz Campus, University of Tehran, Alborz, Iran

[b] School of Mechanical Engineering, College of Engineering, University of Tehran, P.O. Box 11155-4563, Tehran, Iran

Article history:

Received : 20 December 2014
Accepted : 12 January 2015

ABSTRACT

This study investigated the performance and aeroelastic characteristics of a wind turbine blade based on strongly coupled approach (two-way fluid structure interaction) to simulate the transient FSI[1] responses of HAWT[2]. Aerodynamic response was obtained by 3D CFD-URANS approach and structural response was obtained by 3D Finite element method. Aeroelastic responses of the blade were obtained by coupling those aerodynamic and structural models. The analysis model was validated using the experimental result of performance of NREL phase VI rotor which was conducted by NASA/AMES wind tunnel. Numerical results consist of torque and pressure coefficient in different sections of span (over wind speed of 7 to 15 m/s) which were compared with available experimental results. The present model was also evaluated with results of other aeroelastic simulations.

Keywords: Aeroelastic, CFD, FSI, Wind Turbine.

1. Introduction

In order to make wind power industry competitive with the other sources of energy, there is need to decrease the cost of power production of each unit, i.e. increasing diameter of wind turbine blade is one way of reaching this goal. Accordingly, size of commercial wind turbines through the last three decades has increased from 10 *m* (kW class) to more than 120 *m* (MW class). As the diameter of wind turbine increases, aeroelastic phenomenon becomes more important. This phenomenon makes the analysis more complex and the rigid calculation is not accurate enough for turbine performance computation.

In order to make robust aeroelastic analysis, both aerodynamic and structural model must be quiet accurate and robust. Most of the previous aeroelastic computations have used simple methods for aerodynamic and structural model such as blade element momentum method (BEM) by Glauert [1]. The problems associated with these methods are that the structural deflection of blade only considers changing in angle of attack due to twist of the blade section; However, changing in radial flow due to flap wise and edge wise deflections were ignored.

Therefore, aerodynamic loads such as torque are calculated from aerodynamic coefficient of the airfoil section which is constant, and structural deflection is estimated by assumption of constant aerodynamic coefficients. In reality, both the aerodynamic coefficients and the blade sections are changing simultaneously [15, 21].

*Corresponding author: Amir Nejat
Address : Assistant Professor, School of Mechanical Engineering, College of Engineering, University of Tehran, P.O. Box 11155-4563, Tehran, Iran
E-mail address: nejat@ut.ac.ir

[1] Fluid Structure Interaction
[2] Horizontal Axial Wind Turbine

In two-way fluid structure interaction, a CFD solver is used along with dynamic mesh to calculate aerodynamic loads of deflected blade in each time step. This study applies a robust approach for aeroelastic analysis of a wind turbine based on strongly coupled algorithm to simulate the transient FSI responses of HAWT. Aeroelastic responses of blade were obtained by coupling 3D CFD-URANS approach for aerodynamic and FEM method for structure model.

Validation test case was provided by NREL Phase VI unsteady aerodynamic experiment [2, 3, 4] for 3D CFD analysis. This test was performed in The NASA-Ames Research Centre's National Full-Scale Aerodynamics Complex (NFAC) which is the one of the largest world wind tunnel. Numerous researchers have investigated aerodynamic performance of NREL phase VI numerically, using different types of CFD methods and grid topologies without aeroelastic effects [5, 6, 8, 9, 10, 11, 12]. But for aeroelastic analysis, smaller numbers of research works have been conducted. Chaviapolus [13] in 1999 performed linearized aeroelastic analysis; he coupled 3D structural solver to 2D CFD solver for different sections of blade and calculated the aerodynamic force for each section. Y.H. Zhao [14] used unsteady vortex lattice model, to study nonlinear aeroelastic behavior of airfoil. Abianaki and Nejat [15, 21] performed a simple and robust aeroelastic analysis for 2D wind turbine blade by coupling the XFOIL [24] aerodynamic software and the MATLAB PDE toolbox for solving plane stress equation for structural responses. They showed that in elastic model of airfoil, the lift and drag coefficients were lower compared with the rigid airfoil. Gebrad [16] studied aeroelastic responses of wind turbine and captured different aeroelastic phenomena like flutter by coupling unsteady lattice vortex method and 3D finite element solver. Jong-Won Lee [17] performed aeroelastic analysis for NREL5 Megawatt wind turbine by coupling Modified Strip Theory for aerodynamic and 3D finite element solver and reported the performance of the elastic wind turbine. Bazilevs [24, 25] in 2011 conducted a fluid-structure interaction (FSI) procedure for NREL 5 MW wind turbine by coupling a FEM and CFD solvers. The structural solver was based on the isogeometric rotation-free Kirchhoff-Love composite shell and the bending strip method. YuweiLi [26] in 2014 performed FSI simulation using coupled computational fluid/ multibody dynamics. They compared rigid and flexible models for NREL 5 MW. Carrión [27] in 2014 performed aeroelastic analysis on NREL phase VI wind turbine by coupling the compressible flow solver(HMB2) and modal analysis method for structural responses.

Nomenclature

Cp	Pressure confident
ρ	density
ρ_∞	Far field density
V_∞	Far field wind velocity
P_∞	Far field pressure
P	Pressure

2.Fluid Structure Interaction (FSI)

FSI is a combination of structural and fluid flow fields. Those fields are connected by an interface called wet surface where aerodynamic forces act on flexible structure. Those aerodynamic forces cause structural deflection and change of the boundary of fluid domain resulting in the change of flow pattern. New boundary of fluid needs new mesh generation via adapting dynamic boundary method with re-meshing the geometry in each time step. Two main strategies for FSI solution are monolithic and partitioned methods. In monolithic, all structural and fluid flow equations are solved simultaneously. In partitioned strategy, structure and fluid domain are solved iteratively by two different solvers. In one way, the aerodynamic part is solved and the aerodynamic forces are reported to the structural solver; the stresses and deflections in structure are computed as the second part. However, in two ways coupling, the deflection is sent back to fluid solver and a new grid is generated for new boundary of deflected blade. Again calculation of aerodynamic forces and the resulting deflections are repeated in a loop until a convergence criteria is satisfied.

In this project, two ways partitioned fluid structure interaction was used, data transfer between fluid solver and structural solver is shown in Fig.1.

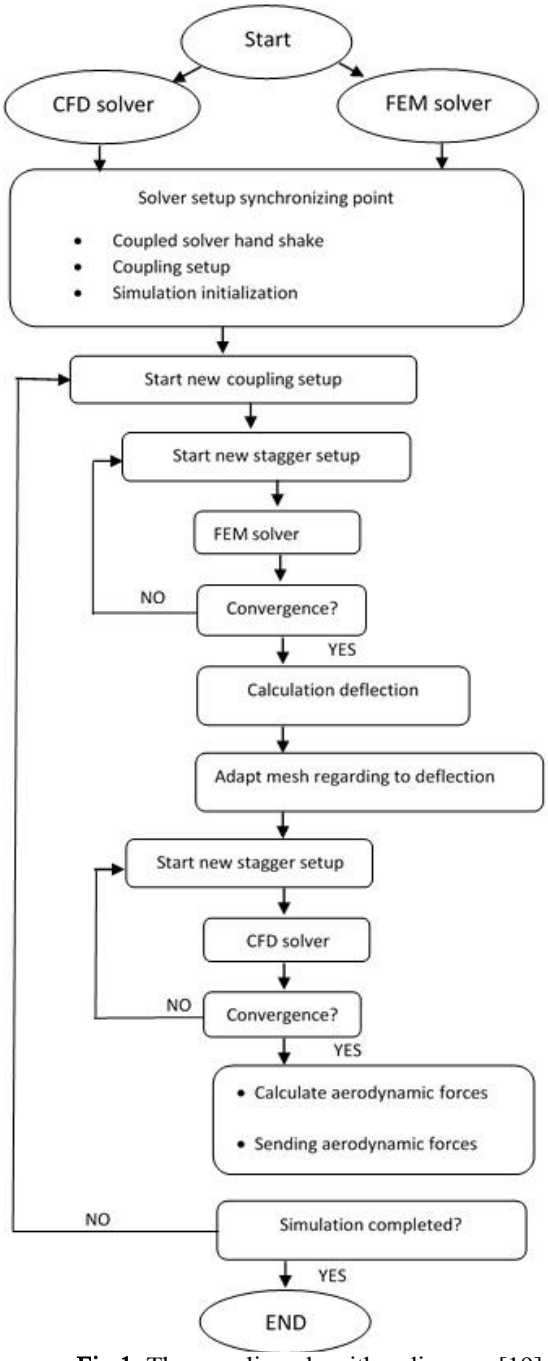

Fig.1. The coupling algorithm diagram [19]

3.Methodology

3.1.FSI Modelling of NREL Phase VI Rotor

A commercial Navier-Stokes CFD solver, CFX, was utilized to compute the flow field for the phase VI rotor. The Solver uses finite-volume discretization with a second order advection scheme [18]. The computations have been performed using Reynolds Averaged Navier- Stokes (RANS) equations and the SST turbulence model; for more details one may refer to the CFX user guides [18-19].

Wind turbine has a power rating of 20 kW, it consists of two blades of 5.029 *m* in radius (the Blades are twisted and tapered). The S809 airfoil is used for the blade out board and for the blade root. For twist and chord information, one may refer to Ref. [2]. Performance of wind turbine blades were measured for wind speeds for a range of 7 to 15 *m/s*, a yaw angle of 0°, pitch angle of 3° and 72 *rpm* rotational speed of the rotor. Operational conditions such as density were 1.233 kg/m^3 for the test. As the turbine is an upwind type, exclusion of tower in the CFD model has negligible effect on rotor aerodynamics [24, 22].

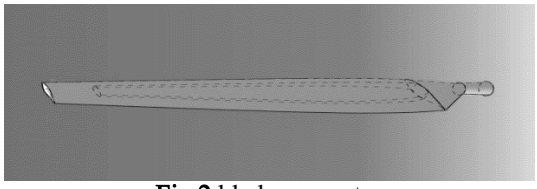

Fig.2.blade geometry

Structural properties of Blade along the span are well documented in Fig.2.

In order to reduce computing cost, a single blade is modeled in CFD by using periodic boundary conditions that is equivalent to 180° periodic sector of the rotor and the final torque result is multiplied by a factor of two.

All CFD simulations have been performed with commercial CFD package ANSYS CFX version 14.0.

3.2.Computational Mesh Grid

Unstructured mesh with prism layer near wall of blade with distance of 0.0001 m as the first layer has been used for the boundary layer grid, as seen in Fig.3. The y^+ is less than 2 for the entire blade in order to accurately calculate the viscose forces near the wall. After performing the mesh independence study, a mesh of 4,176,132 elements was employed for numerical simulation as seen in Figs.3a to 3b.

3.3.Boundary Condition and Setting

At the inlet of domain velocity inlet boundary condition and for the outlet and the far field, pressure outlet boundary conditions are set. The blade surface and hub were defined as no slip walls. Figure 4 shows the different types of boundary conditions that were used in numerical simulation. Selecting the time step for this simulation is crucial and it is affecting the convergence rate of simulation. The time step is chosen in such a way that mesh deformation for each time step remains within a predefined length scale; after trying different time steps, 0.001 s was chosen for this simulation.

3.4.Structural Model

In order to obtain structural response, ANSYS Transient Structure solver was employed. The

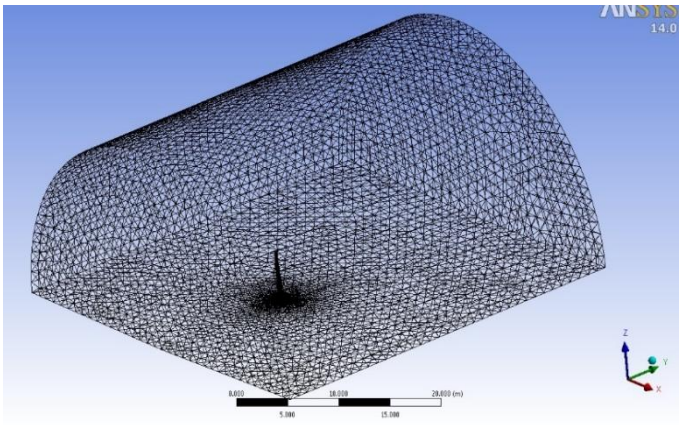

Fig.3. a) Computational mesh

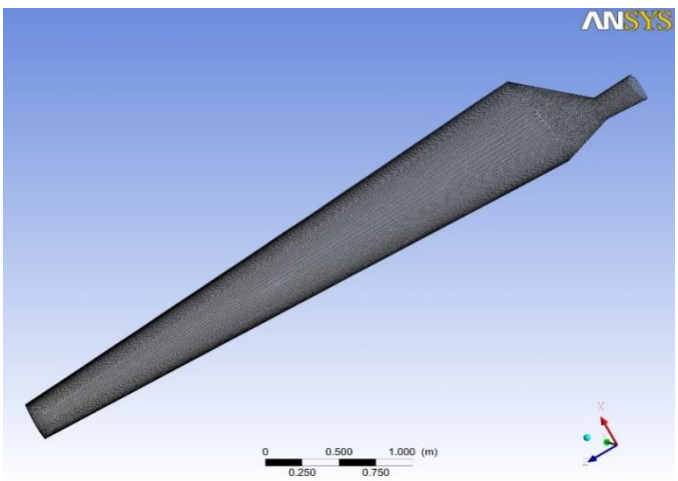

Fig.3. b) Computational mesh and blade

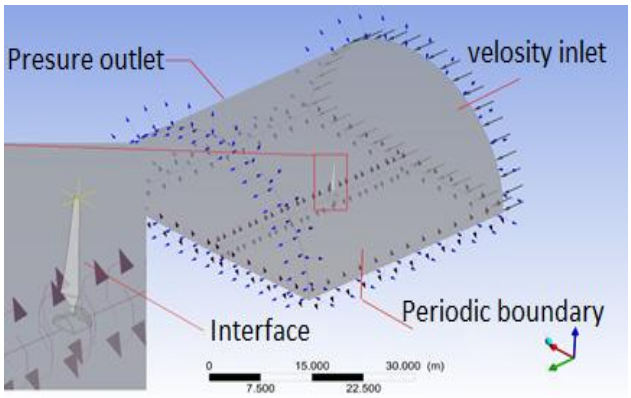

Fig. 4. Computational domain, boundaries and blade

solver uses Finite Element model which is suitable for complex geometries that work under bending, twisting and tension or compression. Mechanical property in span-wise of the blade is changing in span and is reported in Zahle *et al.* [1]. In order to find an equivalent mechanical property in span wise of the NREL Phase VI blade, a solid blade (stiffer than real one) is first generated, then, by using "super position rule", a cross section inner-subpart was subtracted from the initial solid blade in such a way that our blade becomes equivalent of the NREL Phase VI blade. The mechanical properties are reported in Table 1.

4.Results

After mesh generation and setting the flow solver parameters as mentioned in the methodology section in details, the flow field around the wind turbine blade was simulated using two-way FSI model. The mechanical torque (T) was calculated by taking moment of the forces inserted on the solid surface of the blade about the flow axis. The unsteady simulation was continued until the torque residual reduces by 3 orders of magnitude. However, the deflections (flap wise, edge wise and twist wise, i.e. change in angle of attack) were reported at a single time step. The torques of the rigid and flexible models was reported with the same mesh and solver setting and their results were compared with the available experimental data in Fig.5.

It was observed from Fig.5 that the flexible model has followed a consistent trend in predicting torque according to experimental results for different wind speeds. The trend of rigid model is noticeably different as the wind speed increases compared to the experimental and flexible model results where the aeroelastic effects were more present for the wind turbine operation as seen in the Fig.5;

Table 1. Mechanical property along span [21]

Radius	Flap wise EI(Nm^2)	edgewise EI(Nm^2)
0.402	473.517	473.517
0.508	2,320,700	2322100
0.749	1,302,400	1556800
1.006	710,230	1332800
1.257	471,680	1165553
1.509	232,180	997640
2.012	149,420	737010
2.515	123,480	650900
3.018	105,506	583420
3.52	84,468	512420
4.023	65,974	436440
4.526	46,953	387600
5.029	46,953	365070

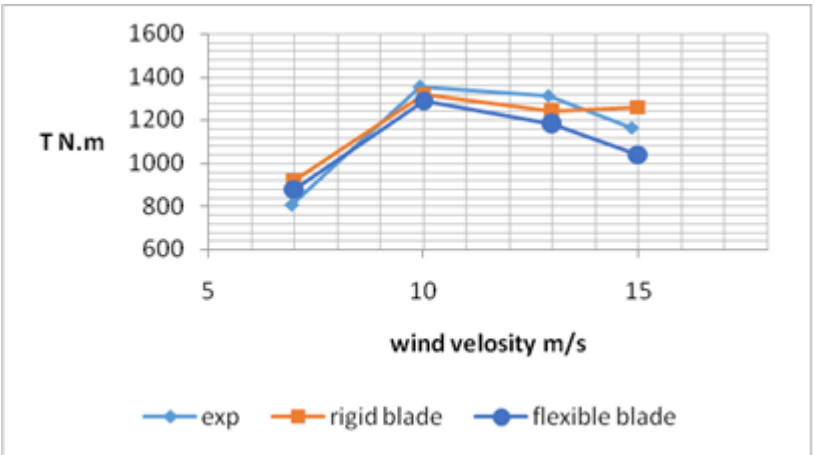

Fig.5. Comparison of flexible and rigid blades torque with experimental measurements

especially in 15 *m/s* wind speed the rigid model has predicted a higher torque. Decreasing angle of attack due to elastic twisting of the blade is the main reason for lower torque shown in Fig.7c for 13 m/s.

Flapwise displacement which causes change in pressure distribution on blade is shown in Figs.6a to 6d for the blade tip for different wind speeds.

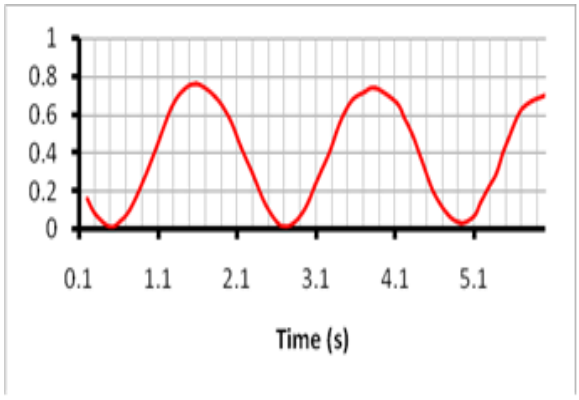

Fig. 6. a) Tip displacement of the blade for flapwise (dm) 7 m/s

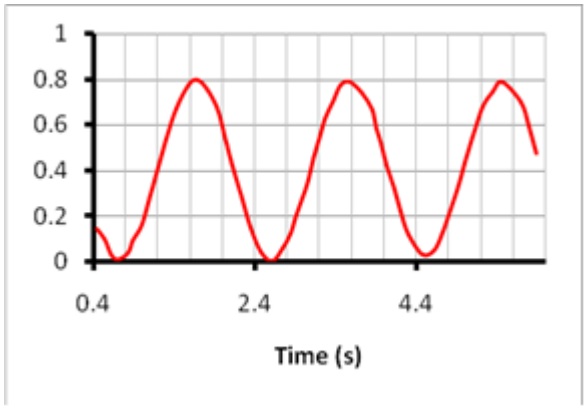

Fig. 6. b) Tip displacement of the blade for flapwise (dm) 10 m/s

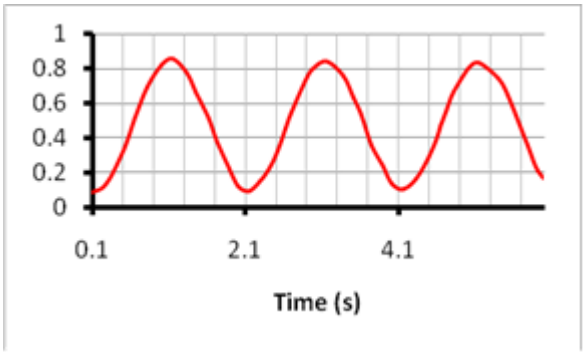

Fig. 6. c) Tip displacement of the blade for flapwise (dm) 13 m/s

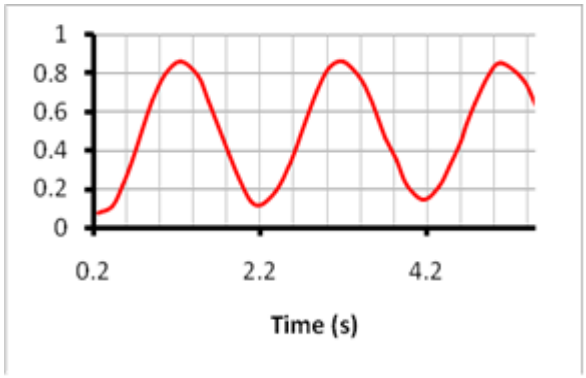

Fig. 6. d) Tip displacement of the blade for flap wise (dm) 15 m/s

It is observed that by increasing the wind speed, the period of flap wise displacement is decreased slightly and the magnitude of the displacement is increased moderately. In 15 *m/s* wind speed, the highest tip displacement was noted near 9 *cm* which is about 2% of the blade radius. It should be mentioned that for a 5 *m* radius turbine blade, these aeroelastic effects are moderate overall, however, for a large wind turbines with more 50 *m* radius these deflections will be quite considerable.

The critical location of blade in bending is the root of blade undergoing the highest stress. Structural design consideration is revised after aeroelastic computation which is quite important for large wind turbines. Deflection along the span is shown in Figs.7a to 7c for 13 *m/s* wind speed. In Fig.7c, the angle of attack is computed using velocity triangles and is compared with the angle of attack of rigid model.

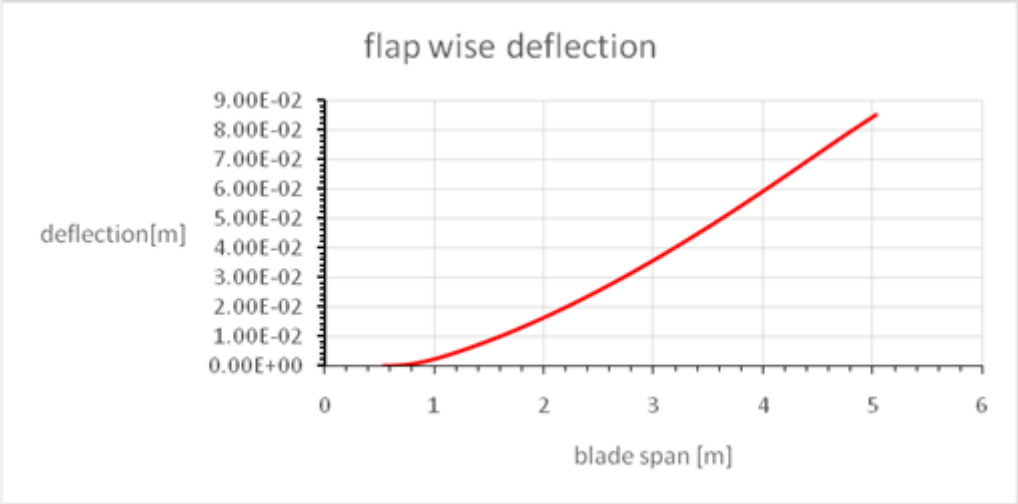

Fig.7. a) Deflection of blade along span in flapwise direction for 13 m/s wind speed

Fig. 7. b) Deflection of blade along span in edgewise direction for 13 m/s wind speed

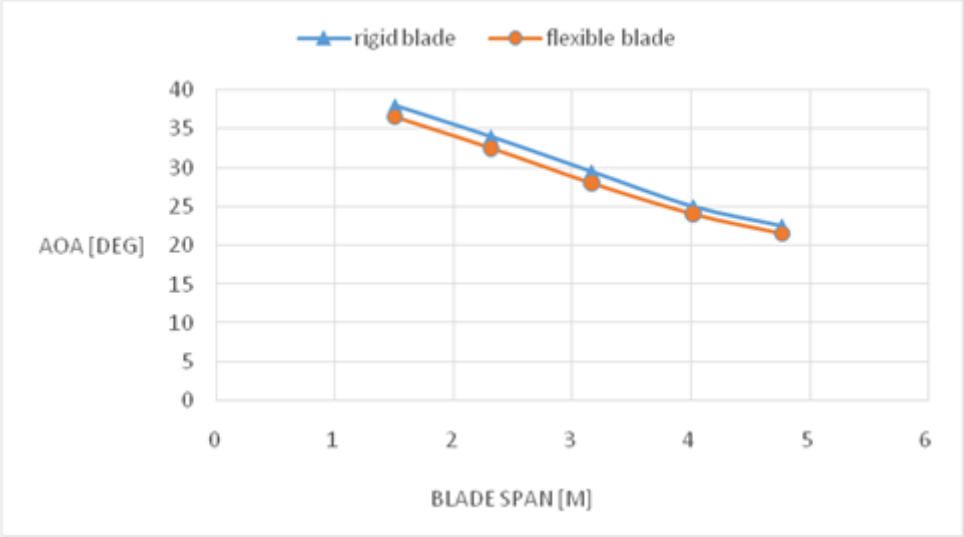

Fig. 7. c) Angle of attack comparison between rigid model and flexible model

It is obvious that the flap wise deflection is larger in magnitude than the edge wise deflection as mechanical stiffness in edge wise is more than flap wise. Deflection along the span behaves like a cantilever beam exposed to distributed load which is a practical and simplified model for aeroelastic computation.

Figure 8 shows the comparison of our aeroelastic results with other aeroelastic predictions for the NREL Phase VI wind turbine. NREL allocated results of different aeroelastic computing sources for predicting NREL phase VI wind turbine performance [20], the aeroelastic results were compared with other results mentioned in Fig.8.

It seems that the presented results are reasonably closer to the experimental data compared with the other approaches results.

Flow field streamlines over the blade surface are depicted in Fig.9.

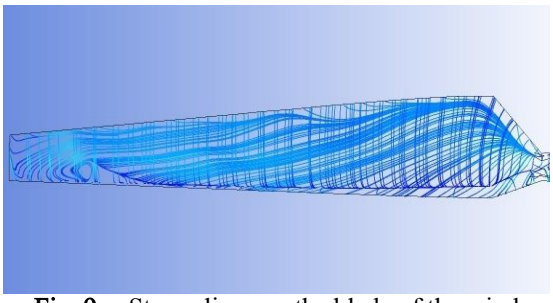

Fig. 9. Streamlines on the blade of the wind turbine model

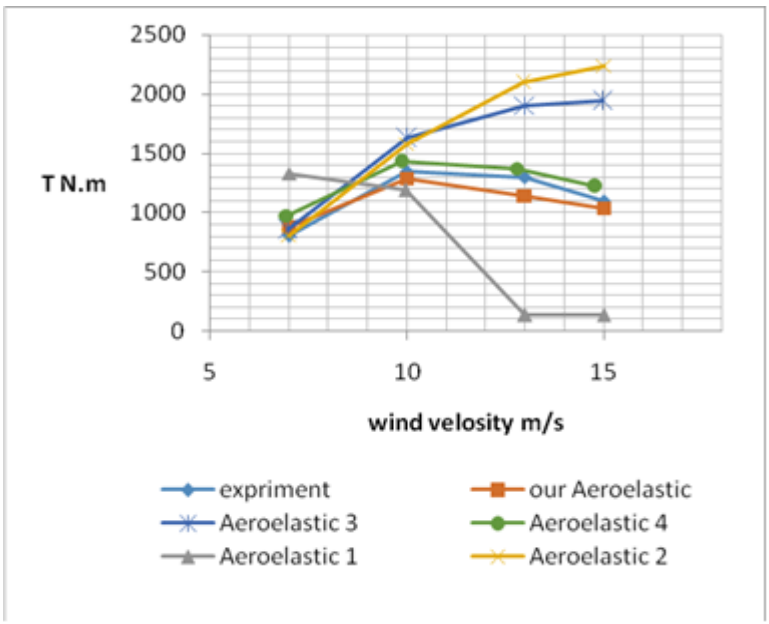

Fig. 8. Comparison of the present results with results of other aeroelastic models

Stagnation line in pressure side and strong radial flow in suction side are clearly obvious; a more interesting phenomenon is the tip vortex flow occurring at the suction side near blade tip reducing the performance of the turbine blade.

4.1.Comparison of span-wise sectional data

Since the experiment pressure measurements are available at five span-wise sections at 30, 46.7, 63.3, 80 and 95% r/R. The pressure coefficient comparison is made between computed flexible results in this study and available experimental data. Cp is defined as Eq.1.

$$C_p = \frac{P - P_\infty}{0.5 \times \rho_\infty \times \left({V_\infty}^2 + (r\omega)^2\right)} \qquad (1)$$

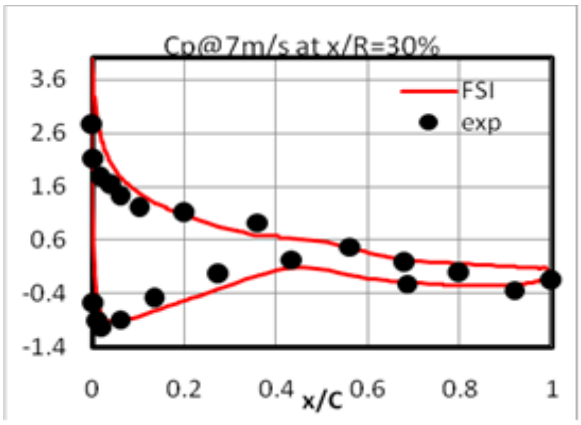

Fig. 10. a) Comparison of FSI and measured pressure distributions at 7 m/s wind speed at 30% of span

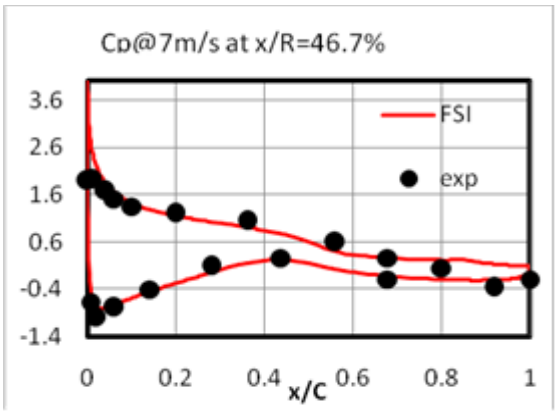

Fig. 10. b) Comparison of FSI and measured pressure distributions at 7 m/s wind speed at 46.7% of span

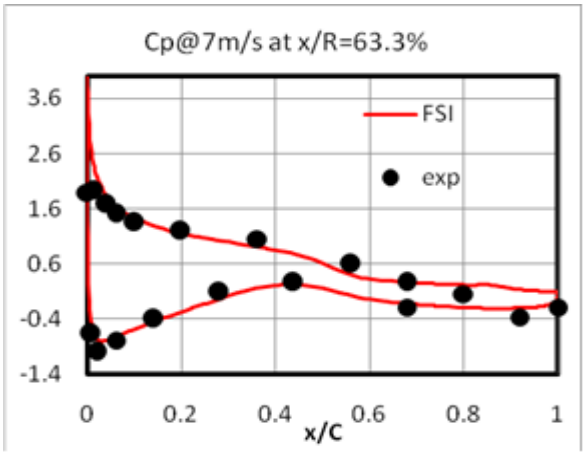

Fig. 10. c) Comparison of FSI and measured pressure distributions at 7 m/s wind speed at 63.3% of span

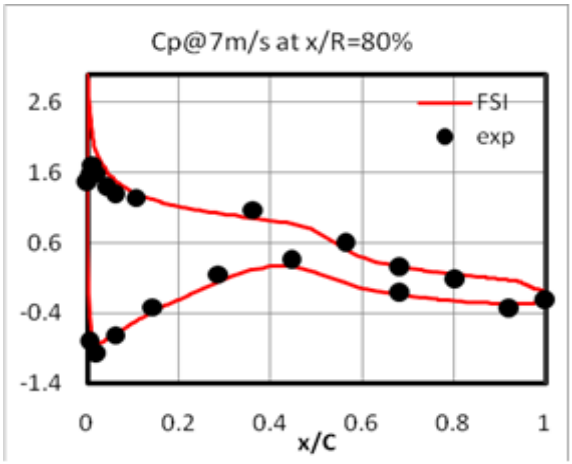

Fig. 10. d) Comparison of FSI and measured pressure distributions at 7 m/s wind speed at 80% of span

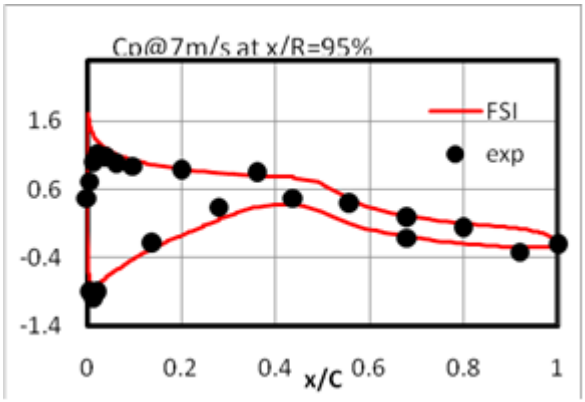

Fig. 10. e) Comparison of FSI and measured pressure distributions at 7 m/s wind speed at 95 % of span

5. Conclusions

This study presented a two-way aeroelastic methodology for wind turbine blade using Finite element method for structural analysis and a commercial CFD solver for flow field computation. The results of this flexible model were verified against experimental data for NREL phase VI experimental data. It was observed that by increasing the wind speed, the period of flap wise displacement was decreased slightly and the magnitude of the displacement was increased moderately. The flap wise deflection was considerably larger in magnitude than the edge wise deflection as mechanical stiffness in edge wise is larger than flap wise. The angle of attack of sections of a flexible model was lower compared to the rigid model reducing the performance of a flexible model due to aeroelastic effects. This study was conducted on a relatively small wind turbine; however as future work the authors intend to apply their validated approach for a NREL 5 MW wind turbine for which the aeroelastic phenomenon will be quite significant.

References

[1] Glauert, Airplane propellers. In Durand, WF (ed.) Aerodynamic Theory, 4th edition, (1935) 169–360. Springer.

[2] Sørensen N. N., Michelsen J. A., Schreck S., Navier-Stokes Predictions of the NREL Phase VI rotor in the NASA Ames 80ft x120 ft wind tunnel, Wind Energy, Vol. 5, No. 2-3, (2002) 151-169.

[3] Hand M.M., Simms D.A., Fingersh L.J., Jager D.W., Cotrell J.R., Schreck S., Larwood S.M., Unsteady Aerodynamics Experiment Phase VI: Wind Tunnel Test Configurations and Available Data Campaigns, NREL/TP-500-29955 (2001).

[4] Larsen J., ANSYS CFD Applied to Wind Turbines at Siemens Wind Power, ANSYS Conference (2008).

[5] Yelmule M. M., Anjuri E., CFD Predictions of NREL Phase VI Rotor Experiments in NASA/AMES Wind Tunnel, International Journal of Renewable Energy research, Vol.3, No.2(2013).

[6] LePape A., Gleize V., Improved Navier-Stokes Computations of a Stall-Regulated Wind Turbine Using Low Mach number Preconditioning, 44th AIAA Aerospace Sciences Meeting and Exhibit, Reno, Nevada,(2006) AIAA 2006-1502.

[7] Duque E. P. N., Burklund M. D., Johnson W., Navier-Stokes and Comprehensive Analysis Performance Predictions of the NREL Phase VI Experiment, Journal of Solar Energy Engineering, (2003)125: 457-467.

[8] Chao D. D., Dam van C. P.,Computational Aerodynamic Analysis of a Blunt Trailing-edge Airfoil Modification to the NREL Phase VI Rotor, Wind Energy, (2004)10:529-550.

[9] Gonzalez A., Munduate X., Three-Dimensional and Rotational Aerodynamics on the NREL Phase VI Wind Turbine Blade, 45th AIAA Aerospace Sciences Meeting and Exhibit, Reno, Nevada,(2007) AIAA 2007-0628.

[10] Schmitz S., Chattot J., Application of a 'Parallelized Coupled Navier-Stokes/Vortex Panel Solver' to the NREL Phase VI Rotor, 43rd AIAA Aerospace Sciences Meeting and Exhibit, Reno, Nevada, (2003) AIAA 2003-0593.

[11] Zahle F., Johansen J., Sorenson N., Wind Turbine Rotor-Tower Interaction Using an Incompressible Overset Grid Method, AIAA 45th Aerospace Sciences Meeting and Exhibit, Reno, Nevada,(2007) AIAA 2007-0425.

[12] Simms D. A., Schreck S., Hand M., Fingersh L., NREL Unsteady Aerodynamics Experiment in the NASA Ames Wind Tunnel: A Comparison of Predictions to Measurements, (2001) NREL/TP-500-29494.

[13] Chaviaropoulos P. K., Flap/Lead –Lag Aeroelastic Stability of Wind Turbine Blade Sections, wind energy journal, 2,(1999) 99-112.

[14] Zhao Y.H, Hu H. Y., Aeroelastic Analysis of a Non-Linear Airfoil Based on Unsteady Vortex Lattice Model, Journal of Sound and Vibration, 276, (2004) 491-510.

[15] Abianaki M. R., Nejat A., Aeroelastic Computation of Awind Turbine Blade Profile, Proceedings of the ASME 2012 International Mechanical Engineering Congress & Exposition(2012).

[16] Gebrad C.G., Roccia B.A., Non-Linear Aeroelasticity: An Approach to Compute the Response of Three-Blade Large-Scale Horizontal-Axis Wind Turbines, Journal of Renewable Energy(2014).

[17] Lee J. W., Lee J. S., Han J. H., Shin H. Ki., Aeroelastic Analysis of Wind Turbine Blades Based on Modified Strip Theory, Journal of Wind Engineering and Industrial Aerodynamics, 110 (2012) 62–69.

[18] Technical Information Regarding the ANSYS-CFX solver, ANSYS CFX-SOLVER Modeling Guide, release 12.1(2009).
[19] Technical Information Regarding the ANSYS-CFX solver, ANSYS CFX-SOLVER Theory Guide, release 12.1(2009).
[20] Hand M.M., Simms D.A., Fingersh L.J., Jager D.W., Cotrell J.R., Schreck S., Larwood S.M., NREL Unsteady Aerodynamics Experiment in the NASA-Ames Wind Tunnel: A Comparison of Predictions to Measurements, technical report, (2001) NREL/TP-500-29955.
[21] Nejat A., Abenaki M., rahbari i., A Robust Engineering Approach for Wind Turbine Blade Profile Aeroelastic Computation, Journal of Energy Equipment and System (2014).
[22] Anjuri E., Comparison of Experimental results with CFD for NREL Phase VI Rotor with Tip Plate, Journal of Renewable Energy Research (2012).
[23] Drela M., XFOIL: An analysis and Design System for Low Reynolds Number Airfoils, Conference on Low Reynolds Number Airfoil Aerodynamics, University of Notre Dame (1989).
[24] Bazilevs Y., Hsu M-C., Akkerman I., Wright S., Takizawa K., Henicke B., Spielman T., Tezduyar T. E., 3D Simulation of Wind Turbine Rotors at Full Scale. PartI: Geometry Modeling and Aerodynamics, International Journal for NumericalMethods in Fluids, 65 (1-3) (2011) 207–35.
[25] Bazilevs Y., Hsu M-C., Kiendl J., Wüchner R., Bletzinger K-U., 3DSimulation of Wind Turbine Rotors at Full Scale. Part II: Fluid-Structure Interaction Modeling with Composite Blades. International Journal for Numerical Methods inFluids 65 (1-3) (2011) 236–53.
[26] Yuwei Li, Coupled Computational Fluid Dynamics/Multibody Dynamics Method with Application to Wind Turbine Simulations, University of Iowa, PhD thesis(2014).
[27] Carrión M., Steijl R., Woodgate M., Barakos G.N., Munduate X., Gomez-Iradi S., Aeroelastic Analysis of Wind Turbines Using a Tightly Coupled CFD–CSD Method, Journal of Fluid and Structure (2014).